The Astrophysical Journal Letters, 888:L4 (7pp), 2020 January 1 https://doi.org/10.3847/2041-8213/ab5c87

Long-lived Dust Rings around HD 169142

Claudia Toci[1], Giuseppe Lodato[2], Davide Fedele[3], Leonardo Testi[3,4,5], and Christophe Pinte[6]
[1] INAF—Osservatorio Astronomico di Brera, Via Brera 28, I-20121 Milan, Italy; claudia.toci@inaf.it
[2] Dipartimento di Fisica, Universitá degli Studi di Milano, Via Giovanni Celoria 16, I-20133 Milano, Italy
[3] INAF—Osservatorio Astrofisico di Arcetri, Largo E. Fermi 5, I-50125 Florence, Italy
[4] European Southern Observatory Karl-Schwarzschild-Str 2, D-85748 Garching, Germany
[5] Excellence Cluster ORIGINS, Boltzmann-Str. 2, D-85748 Garching, Germany
[6] Monash Centre for Astrophysics (MoCA) and School of Physics and Astronomy, Monash University, Clayton, VIC 3800, Australia
Received 2019 September 25; revised 2019 November 4; accepted 2019 November 15; published 2019 December 27

Abstract

Recent Atacama Large Millimeter/submillimeter Array (ALMA) observations of the protoplanetary disk around HD 169142 reveal a peculiar structure made of concentric dusty rings: a main ring at ∼20 au, a triple system of rings at ∼55–75 au in millimetric continuum emission, and a perturbed gas surface density from the ^{12}CO,^{13}CO, and C^{18}O ($J = 2$–1) surface brightness profile. In this Letter, we perform 3D numerical simulations and radiative transfer modeling exploring the possibility that two giant planets interacting with the disk and orbiting in resonant locking can be responsible for the origin of the observed dust inner rings structure. We find that in this configuration the dust structure is actually long lived while the gas mass of the disk is accreted onto the star and the giant planets, emptying the inner region. In addition, we also find that the innermost planet is located at the inner edge of the dust ring, and can accrete mass from the disk, generating a signature in the dust ring shape that can be observed in mm ALMA observations.

Unified Astronomy Thesaurus concepts: Protoplanetary disks (1300); Planetary system formation (1257); Astrophysical fluid dynamics (101)

1. Introduction

The initial conditions for the formation of planets naturally determine the characteristics of the resulting planetary system (Mordasini et al. 2016) and are connected to the properties of the protoplanetary disks where planet formation occurs. Several substructures within these disks have been imaged in great detail with the Atacama Large Millimeter/submillimeter Array (ALMA) and the Very Large Telescope/SPHERE (e.g., Benisty et al. 2015; Andrews et al. 2018). The most common kind of substructure appears to be in the form of gaps and rings, which play an important role due to their possible connection with ongoing or subsequent formation of planets. Indeed, rings seem to be common and they are found at any distance to the star, with no correlation between their location and the host star luminosity (Huang et al. 2018; Long et al. 2018), but occur with different morphologies (Liu et al. 2019). It is still under debate whether these structures are long lived, and thus represent a feature that is related to an evolutionary stage of the system, or they are transient structures, created and destroyed on shorter timescale compared with the disk lifetime. This question is closely related to the estimate of the age of protoplanetary disks and has important implications on the dust and planetesimal evolution: a long-lived ring can be an ideal environment for grain growth (Brauer et al. 2008). Naturally, their lifetimes are dependent on the mechanism that generates them. Indeed, in order to explain their presence many theoretical models have been proposed, including dead-zone edges (Pinilla et al. 2016), self-induced reconnection in magnetized disk-wind systems (Suriano et al. 2018), photo-evaporation (Alexander et al. 2014), or dust processes (Birnstiel et al. 2015; Gonzalez et al. 2015). Another possibility is that the presence of planets embedded in the disks create pressure bumps in the gas, confining the dust in rings as discussed in Pinilla et al. (2012). The recent discoveries of planets inside gaps, either by direct imaging (Keppler et al. 2018) or by their kinematic signatures (Pinte et al. 2018), and the fact that the location of gaps does not coincide with the expected snow lines (Huang et al. 2018; Long et al. 2018), lends credit to the idea that at least some of these gaps mark the presence of young planets (ALMA Partnership et al. 2015; Dipierro et al. 2015; Lodato et al. 2019). This is supported by the comparison of the direct and indirect detection of candidate protoplanets with synthetic images obtained performing radiative transfer and hydrodynamical simulations (see, i.e., Dipierro et al. 2015). According to current theories, a planet still embedded in its disk should accrete mass and open a partially depleted gap in the circumstellar disk (Crida et al. 2006). The accreted material is expected to orbit around the planet, forming a rotating circumplanetary disk. To date, a few candidates still embedded in their parental circumstellar disks have been claimed (Isella et al. 2019), but most still lack confirmation (Testi et al. 2015).

The young Herbig Ae/Be star HD 169142 has an age of 6^{+6}_{-3} Myr and a mass of $M_\star = 1.65\ M_\odot$. Its distance is 117 ± 4 pc (Gaia Collaboration et al. 2016). According to Panić et al. (2008) observations in the 1.3 mm dust continuum and CO ($J = 2$–1) emission line, the disk has an inclination of 13°, a position angle of 5°, and a total gas mass of ∼0.6–3.0 × 10^{-2} $M_\odot$, confirmed by subsequent observations (Fedele et al. 2017; Pérez et al. 2019, hereafter FD17 and PS19). This source has been observed in the thermal mid-infrared emission (Honda et al. 2012), near-infrared emission (Osorio et al. 2014; Reggiani et al. 2014; Pohl et al. 2017; Bertrang et al. 2018; Ligi et al. 2018), near-infrared polarimetric, and scattered light images (Pohl et al. 2017). Gas and dust are physically decoupled in HD 169142. The source shows two dust rings in continuum emission: an inner one between ∼20 and 35 au, heavily depleted of dust and gas (FD17; Macías et al. 2019, hereafter ME19), and an outer one at ∼55–85 au, recently resolved as a system of three thin

rings by observations of PS19, while CO isotopologous emission maps of FD17 point out that the gas has an inner cavity (∼50 au), with surface density reduced by a factor of ∼30–40 (FD17; ME19).

Many authors (FD17; Pohl et al. 2017; Bertrang et al. 2018; Ligi et al. 2018; ME19; PS19) pointed out the presence of giant planets in the disk ($M >$ few Jupiter masses, hereafter M_J), an inner one located inside the inner dust cavity ($R < 20$ au), and an outer one in the gap between the two dust rings ($35 < R < 55$ au) to explain the signature double-ring morphology. The splitting of the outer ring in concentric rings have been modeled by PS19 with the presence of a single migrating low-mass planet ($\sim 10^{-2}$ M_J). Potential signatures due to the presence of a candidate massive protoplanet could have been detected in this source via direct imaging in the radio/near-infrared (Reggiani et al. 2014; Ligi et al. 2018; Gratton et al. 2019), but the nature of the candidates still have to be confirmed.

In this Letter we model the two prominent dust rings and tmehe cavity of HD 169142, including in the system of two giant planets, in order to check whether this substructure is a transient or is actually a long-lived feature, giving constraints on the ratio between the masses and the position of the planets. We present the results assuming a single value for the gas and dust mass of the protoplanetary disk, showing that we can obtain a long-lived dust ring trapped between two giant planets with resonant orbits. In a forthcoming paper we will present a more general study on this mechanism.

2. Hydrodynamical Simulation

We perform 3D global simulations of dust and gas disk with two embedded giant protoplanets using the smoothed particle hydrodynamics (SPH) code PHANTOM (see Lodato & Price 2010; Price et al. 2018). We assume a single grain size of 1.00 mm, employ the single-fluid algorithm based on the terminal velocity approximation (Laibe & Price 2014). The conservation of the dust mass is granted due to the prescription of Ballabio et al. (2018).

We consider a star with mass 1.65 $M_\odot$ and two planets allowed to migrate and accrete mass. They are initialized at a location of 18 and 55 au and with masses of $M_1 = 1.5$ M_J and $M_2 = 0.5$ M_J respectively, so that $M_2/M_1 < 1$ initially. They are massive enough to open a gap in the gas surface density according to Crida et al. (2006) but are initially smaller in masses and further out in position with respect to previous models (see i.e., Pohl et al. 2017), in order to account for the accretion of dust and gas and the migration of planets during the simulation. Our time unit is the period of the outer planet at its initial position (55 au, $T_{orb} \sim 320$ yr).

We represent the protoplanetary bodies and the central star using sink particles (Bate et al. 1995) with accretion radii of one-eighth of the Hill radius (Dipierro et al. 2015) for the planets (0.14 and 0.4 au, respectively). For the central star, due to the fact that our aim is to model the gas and dust dynamics at ∼20 au, we chose an accretion radius of 5 au, not considering the innermost part of the disk behavior. We also tested our results for an accretion radius of 1 au, finding no significant differences. We chose not to include a third body (as predicted by PS19), used to model the outer ring splitting. As already stated, our aim is to characterize the inner structure as a function of the two giant planets. Dust and gas can be accreted onto the sinks, representing a condition that mimics a real accretion scenario and the planets are free to migrate due to planet–disk interaction, planet–planet interaction, and viscous disk evolution. Thus, in our simulations all the material that enters the sink radius is considered as instantaneously accreted. This may overestimate the accretion onto the planet, and we remark that in the following, when we refer to the "planet mass," this should actually be considered as the mass of the planet and of its circumplanetary disk.

We set up the disks in PHANTOM using the setup from Lodato & Price (2010). The scenario is modeled with the central star surrounded by a disk of 10^6 SPH particles, extending from $R_{in} = 5$ to $R_{out} = 150$ au. The surface density profile $\Sigma(R)$ is

$$\Sigma(R) = \Sigma_0 \left(\frac{R}{R_0}\right)^{-p} \exp\left[-(R/R_0)^{(2-q)}\right]\left(1 - \sqrt{\frac{R_{in}}{R}}\right), \quad (1)$$

where $R_0 = 100$ au, p and q are two indexes, and the density normalization $\Sigma_0 = 3.6$ g cm^{-2} is set to have an initial total gas mass of $\sim 10^{-2} M_\odot$. We assume a locally isothermal equation of state where the sound speed profile is $c_s = c_{s,ref}(R/R_{ref})^{-q}$. The aspect ratio in the gas is given by $H/R = (H/R)_{ref}(R/R_{ref})^{(1/2-q)}$. We also assumed an aspect ratio value of $H/R = 0.07$ at $R = R_{ref}$ and $p = q = 0.5$ as found in FD17. We set the SPH α_{AV} viscosity to obtain an effective Shakura & Sunyaev (1973) viscosity $\alpha_{SS} = 0.005$.

The initial dust mass is 1.2×10^{-4} $M_\odot$, close to the value found by FD17 based on the 1.3 continuum observation. The dust surface density has initially the same functional form of the gas, but is scaled down assuming a gas-to-dust ratio of 80 as inferred from FD17 CO isotopologous measurements. For our chosen dust size of $a = 1$ mm (and assuming an internal density of the dust of $\rho_d = 3$ g cm^{-2}), the initial Stokes number, defined as $\sim S_t = \rho_d a/\Sigma_{gas}$, is smaller than 1. This implies that dust and the gas are initially coupled in the disk.

2.1. Radiative Transfer Model

To directly compare (Pinte et al. 2006) with observations of HD 169142 we post-process our simulation using the Monte Carlo radiative transfer code MCFOST (Pinte et al. 2009). The code directly maps from the SPH particle to the radiative transfer grid physical quantities such as density and temperature thanks to a Voronoi tesselation that matches each cell with an SPH particle, without any interpolation. The astronomical silicates and carbons are assumed from Draine (2003). The grain size distribution has a slope of −3.5 and goes from 0.03 μm to 3 mm. To irradiate the disk the star is treated as an isotropic source with stellar spectral models obtained from the 5 Myr isochrones from Siess et al. (2000), with $T_{eff} \sim 8000$ K and a radius $R \sim 2.2$ $R_\odot$. The source is located at the distance of 117 pc, adopting the disk inclination and position angle of 13° and 5°.

3. Results

Our reference profile for the gas and dust distributions is the DALI thermochemical model from FD17, that models the dust surface density profile Σ_{dust} with two dust rings (20–35 au and 56–83 au) and the gas density profiles Σ_{gas} with an inner cavity (13–56 au) reduced by a factor 30–40. However, we considered an update of the published model of FD17, limited by the spatial resolution of the available data at the time. Based on the

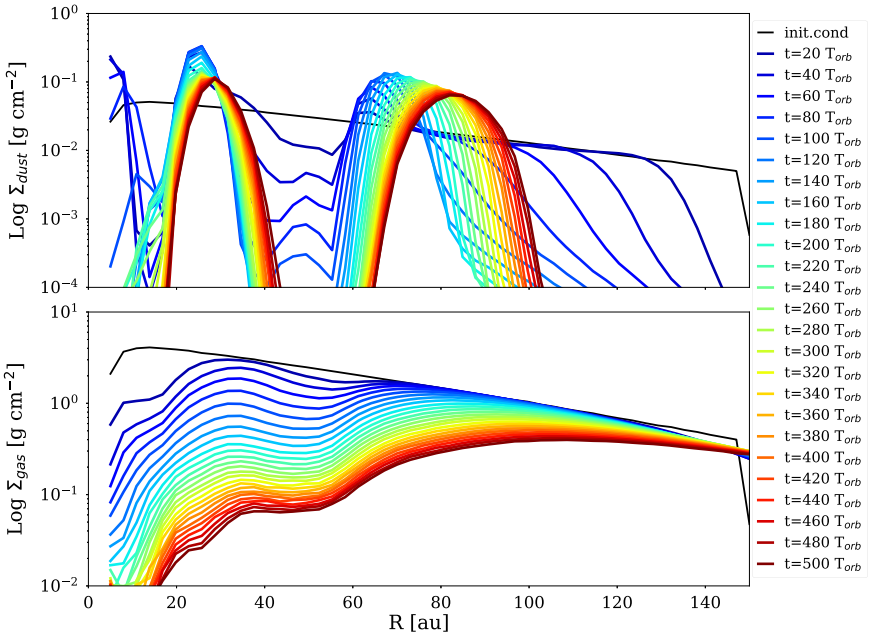

Figure 1. $\Sigma_{\rm dust}$ (top panel) and $\Sigma_{\rm gas}$ (bottom panel) as a function of the radius R for increasing time. The initial surface density profiles are in black. Our time unit is normalized with the initial orbital period of the outer planet (∼320 yr).

^{13}CO $J = 3$–2 ALMA archive data from Honda et al. (2012), the gas cavity appears to be located at ∼20–56 au.

Figure 1 shows the temporal evolution of the dust and gas surface density profiles, $\Sigma_{\rm dust}$ and $\Sigma_{\rm gas}$, in our simulation. Going from black to red, $\Sigma_{\rm dust}$ and $\Sigma_{\rm gas}$ are displayed as a function of time, that we recall is normalized to the orbital period of the outer planet at the initial position (55 au, $T_{\rm orb} \sim 320$ yr).

The inner planet carves a cavity in the dust and in the gas, with a depletion factor of $\sim 10^{-4}$ and $\sim 10^{-1}$, respectively, inward of its orbit. The outer planet first migrates (see Figure 2) while accreting the material, then opens a gap in dust and gas (with depletion factor $\sim 10^{-4}$ and $\sim 10^{-1}$, respectively, in dust and gas) at his "equilibrium" location. The dust ring produced between the two planets is preserved for at least ∼500 orbits, i.e., for over $\sim 2 \times 10^5$ yr. At the same time, the gas is accreted on the star and the planets. The density profiles of the gas and dust in our simulation are due to a combination of factors. For the gas, the "cavity" is produced by the torques exerted by the outer planet onto the disk, which prevents the gas outside the outer planet to refill the inner regions that are emptied by viscous accretion. For the dust, the two prominent rings are created by the usual trapping at pressure maxima (indeed, we have verified that the ring location coincides exactly with pressure maxima). This generates a gas cavity with a width of ∼50 au, lowering the gas surface density and increasing the value of the Stokes number that quickly becomes larger than unity, helping the dust trapping due to the pressure gradient in preventing the dust migration and thus preserving the dust ring.

The outer dust ring is located outside the outer planet and shrinks for dust migration as the disk evolves for the first ∼150 $T_{\rm orb}$. Later on ($t > 200\ T_{\rm orb}$), the dust ring radius increases with time and the ring moves outward as the maximum of the gas pressure moves outward, in agreement with a dust trapping due to pressure bump scenario (Pinilla et al. 2012). As time passes by, the width of the gap grows as the mass of the second planet grows, as expected from Crida et al. (2006) and Dipierro & Laibe (2017). As can be seen in Figure 1, during the process (at

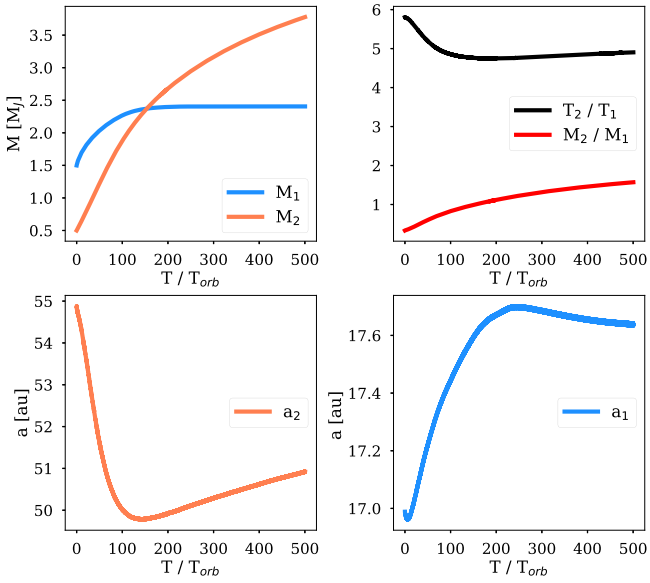

Figure 2. Dynamics of the two planets. Top-right panel: the masses of the planets; top-left panel: the ratio between the outer and inner periods and masses; the orbital semimajor axis of the outer (bottom-left panel) and inner planets (bottom-right panel) as a function of the normalized time.

∼100–200 orbits) the inner edge of the inner ring spreads inward, making the dust surface density profile skewed (compare the green and cyan lines with the blue and red lines, which refer to early and later time, respectively), as found also in PS19.

Figure 2 shows the dynamics of the planets. In the first ∼50 orbits the system relaxes out of the initial conditions: the outer planet rapidly migrates to ∼50 au bottom-left panel), while the inner planet remains at ∼17 au, slowly migrating outward (bottom-right panel). This leads the orbits of the two objects to become in a 5:1 period resonance (top-right panel). Figure 2 also shows the masses of the two planets as a function of time (top-left panel). After the first $\sim 100\ T_{\rm orb}$ the inner planet has

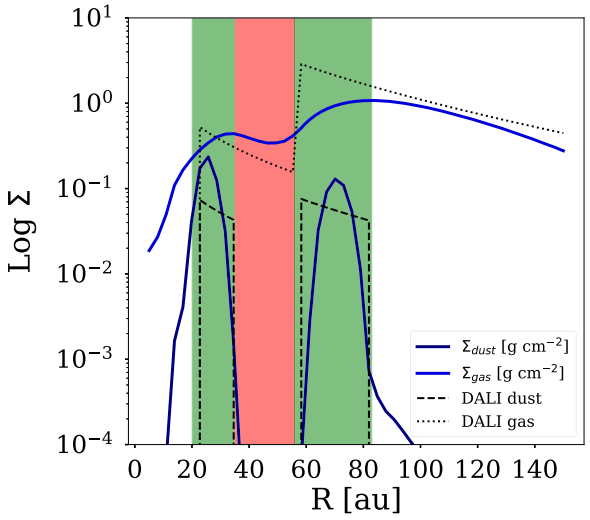

Figure 3. Comparison between the $\Sigma_{\rm gas}$ and $\Sigma_{\rm dust}$ profiles after 160 $T_{\rm orb}$ and the update DALI model of FD17. The green and red regions are the observed locations of the rings and the gap, respectively.

already accreted almost all of the available mass, reaching the value of $\sim$2.5 $M_{\rm J}$, while the outer planet continues to accrete mass from the external ($R > 60$ au) reservoir of gas, overcoming the mass of the inner planet (initially $M_1 > M_2$, while at the end of the simulation $M_2 > M_1$). This leads to a small change in the position of the two planets, the inner actually migrating outward. We underline that, while the outer planet is located almost in the middle of the outer gap, our simulation shows that the inner planet is actually located at the inner edge of the ring. The outward migration of the planet generates the skewness of the ring shown in Figure 1: it is actually dust accreted on the planet via a dusty circumplanetary disk.

Our best agreement with the results of the updated version of the thermochemical model of FD17 is obtained after $160\,T_{\rm orb} = 5 \times 10^4$ yr and it is shown in Figure 3. The total mass of the disk is $\sim 6 \times 10^{-3}\ M_\odot$ and the dust mass is $\sim 0.9 \times 10^{-4}\,M_\odot$. The inner planet is located at $\sim$17.4 au and the outer at $\sim$50 au, with almost equal masses, $\sim$2.4 $M_{\rm J}$.

Figure 4 displays the synthetic observations of our simulation. The first and second rows show, respectively, our model continuum emission at 1.3 mm convolved with a 0.″02 (image (a.1)) and 0.″2 beam (image (b.1)), in good agreement with the observed fluxes of PS19 and FD17 (images (a.2) and (b.2), respectively). The third and fourth rows show 3.1 mm at 0.″16 resolution (image (c.1)) and 0.890 mm at 0.″02 (image (d.1)) simulated observations of our disk, in good agreement with ME19 observations ((c.2) and (d.2), respectively). Our continuum emission images have been obtained supposing a chemical composition for the dust grains of 70% silicates and 30% carbonaceus material, with a porosity level of 10%. Panels (e.1) and (e.2) show the azimuthally averaged profile of our model and PS19, respectively. The ring profile is well reproduced and the value of the flux is consistent with the observation.

An interesting feature of our simulation, as mentioned above, is the creation of a distinct dust feature at the inner edge of the inner ring, probably due to dusty material accreted from the disk disposed around the inner planet in a circumplanetary disk. This is clearly visible also in our simulated ALMA observations in Figure 4. Such a feature might have been already observed, in particular in the high-resolution data of PS19 (see the radially extended feature in their Figure 2, at an angle of $\sim$40°). In order to confirm this hypothesis, one might check the evolution of the feature with time, due to the Keplerian rotation of the inner planet, which has a period of $\sim$60 yr assuming a distance of $\sim$18 au. Figure 5 shows a zoom of the inner part of our model. The top panel refers to simulated ALMA Band 6 observations, while the lower panel refers to ALMA Band 7. From left to right, the plot refers to three different times in the simulations, separated by three years each for Band 6 and two years each for Band 7. Future observations of this system might clearly detect such shift in the azimuthal location of the feature, as the planet is expected to rotate by a 5° angle in one year.

4. Discussion

The presence of two giant planets shapes the disk, explaining the presence of the two rings in the dust and the cavity in the gas. The dust gap quickly opens (after 40–60 $T_{\rm orb}$) due to pure gravitational effects (Crida et al. 2006) and dust radial drift (Dipierro & Laibe 2017). The gas gap opens at slower rate due to the effects of the interaction between the planets and the disk and the viscous evolution of the disk itself. The presence of the planets creates two pressure bumps, where the dust rings are trapped. After $\sim$100–120 $T_{\rm orb}$, due to the high masses of the planets the inner part (with the gas cavity and the dust ring) starts to be disconnected from the outer part, which includes the outer dust ring at $\sim$50–70 au and a reservoir in gas that extends for radii larger than $\sim$150 au.

The outer planet is still accreting material from the gas reservoir, increasing its mass. This interaction between the outer planet and the disk also prevents the refilling of the inner gas gap. However, the star is also accreting material from the inner part of the disk due to viscous accretion. As a consequence, the gas surface density decreases with time, creating a cavity for $R < 50$ au. This reduces the effect of the pressure bump in the inner part of the disk, but increases the value of the Stokes number. The global effect is that the inner dust ring is preserved in time. We do not reproduce the outer ring splitting including a third planet, as this is beyond the scope of the present study, but we note that the interpretation of PS19 (a third planet) is a likely possibility.

The longevity of this configuration allows the formation and migration of outer protoplanets as found in PS19. The dust trapped in the inner region can grow in size, explaining what can be seen in the 3.0 mm observation of ME19. Indeed, we also obtain the absence of dust grains inside the cavity and the gap with a surface density reduction (compared to the assumed initial structure) of $\sim$30–40 and a gas to dust ratio of $\sim$1 as found in FD17 and ME19.

The planetary system displayed in our simulation, with two giant planets in orbital resonances, is a common feature of the observed exoplanetary systems, and is is also present in our solar system. Our simulation also seems to highlight how giant planets tend to reach orbital resonances while still embedded in the parental disk. This fact, combined with the gravitational interaction between them, led in our configuration to a small outward migration of the inner planet that orbits close to the inner edge of the innermost dust ring and not in the center of the cavity as expected. This behavior is not dependent on the initial condition of the planets; it is free to migrate.

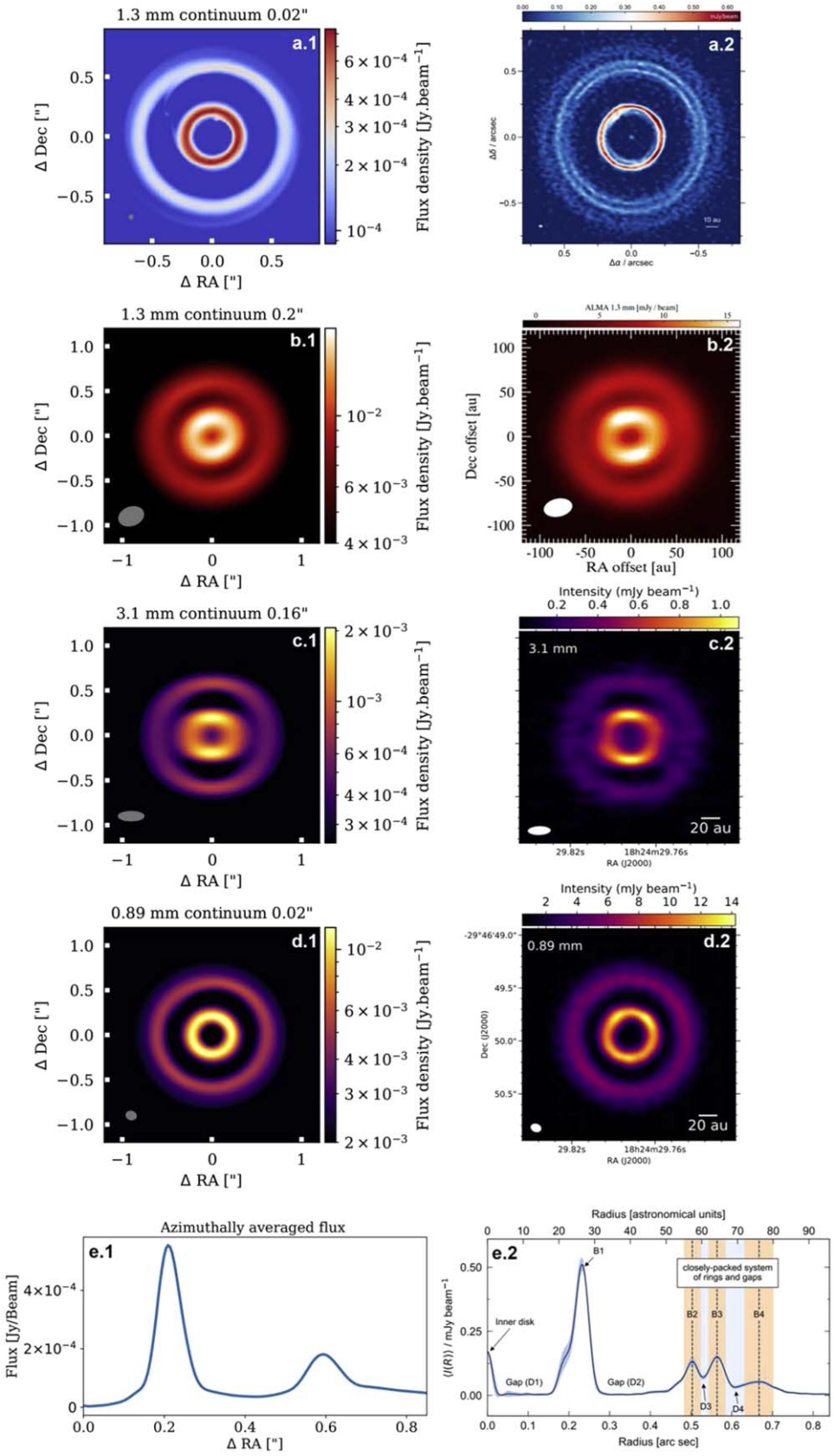

Figure 4. Comparison between simulated observations of our disk model and ALMA observations. (a.1), (b.1), (c.1), (d.1), (e.1): model, (a.2), (b.2), (c.2), (d.2), (e.2): observations from PS19 (1.3 mm continuum emission), FD17 (1.3 mm), ME19 (3.1 and 0.89 mm), respectively. The gray filled ellipse in the bottom-left corner indicates the simulated beam size.

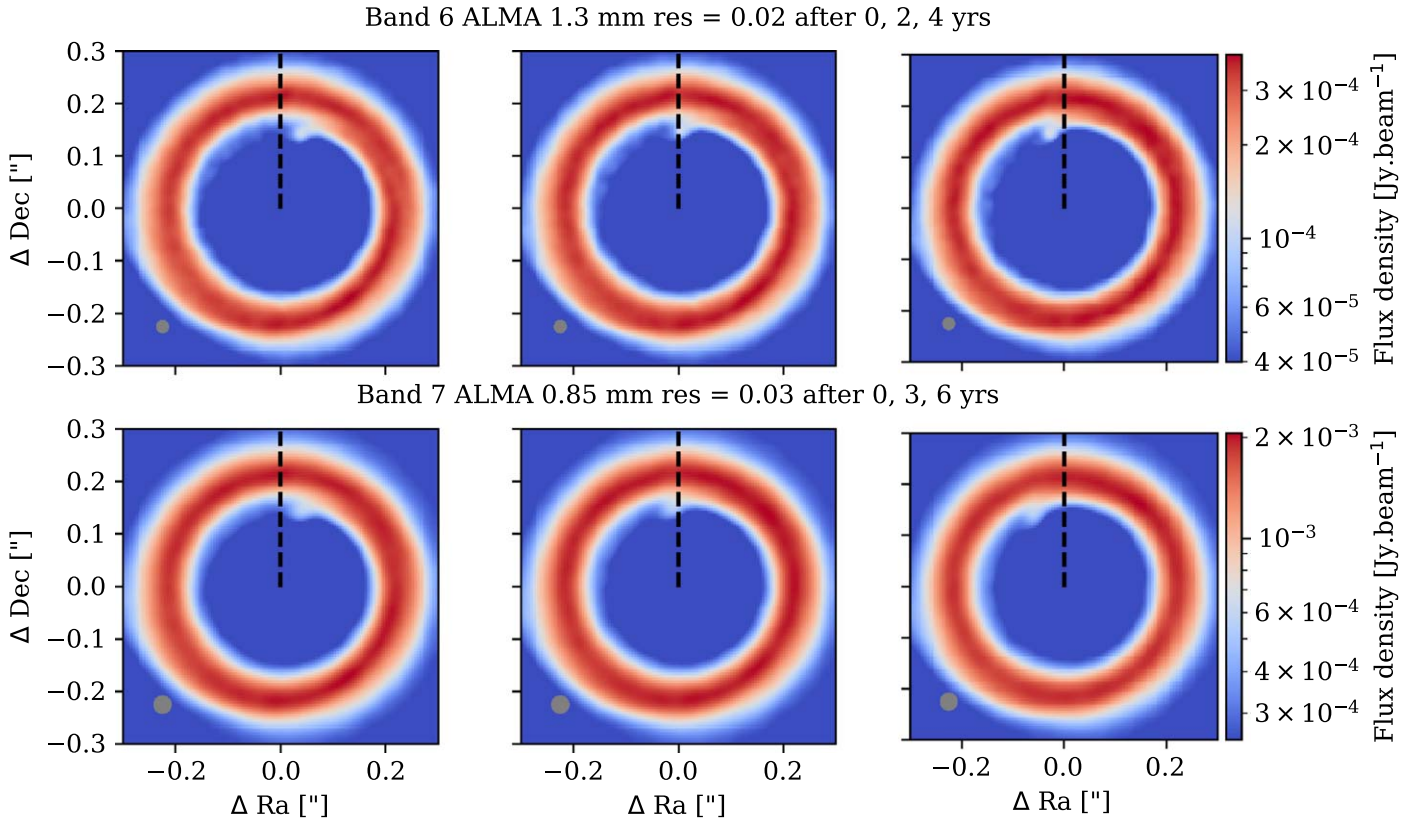

Figure 5. Zoom in of the inner part of the model. The inner planet is located close to the inner edge of the ring, generating an accretion feature visible in our model and expected to move covering ∼5° in ∼1 yr. Top row: ALMA Band 6 observations at three different times separated by three years each. Bottom row: ALMA Band 7 observations at three different times separated by two years each. The gray filled ellipse in the lower-left corner indicates the simulated beam size.

5. Conclusions

We run hydrodynamic simulations and reproduce long-lived dust rings between two giant planets, a scenario that can model the observations of the inner region of the protoplanetary disk HD 169142.

We included two giant planets that are free to migrate, initially not in orbital resonant positions, obtaining our best fit with masses of ∼2.4 M_J at 17.4 and 50 au, in a resonant locking of 5:1. The total mass of the disk is $\sim 6 \times 10^{-3}\ M_\odot$ and the dust mass is $\sim 0.9 \times 10^{-4} M_\odot$.

Our result shows that is possible to form and preserve a dust ring between the orbits of two giant planets for at least $\sim 2 \times 10^5$ yr, a significant fraction of the disk lifetime. The dust is initially trapped in the pressure maximum between the two planets. As the gas surface density decreases inside the gas gap, the value of the Stokes number increases to values larger than unity, helping the pressure bump in preserving the dust to migrate.

The combined effect between the planet–disk interaction and the gas accretion on the planets and the star leads to the shaping of a decreased (at least one order of magnitude) region in the gas surface density profile ($R < 50$ au), as expected from the CO lines observations of FD17. The fact that our code allows the planet to accrete and migrate, reaching minimum energy configurations and resonances, is crucial for obtaining these results.

While the outer planet is located at the center of the gap, the inner one is close to the inner edge of the dust ring and can eventually accrete material from it, generating a feature that might be observable and can explain the ALMA 1.3 mm observation of SP19. Further observations with ALMA are crucial for understanding if this feature is really due to a protoplanet accreting in the cavity.

This configuration is important also for explaining the dynamics of observed cases such as PDS 70 (Keppler et al. 2018), where the outer planet is located at the edge of the dust ring and is actively accreting material. However, in the case of PDS 70 the inner planet has a mass that is larger than the outer one, a situation that is opposite to our scenario.

The authors want to thank the referee for constructive comments that improved the quality of this manuscript. This work and C.T. are supported by the PRIN-INAF 2016 The Cradle of Life—GENESIS-SKA (General Conditions in Early Planetary Systems for the rise of life with SKA). C.T., D.F., and L.T. acknowledge financial support provided by the Italian Ministry of Education, Universities and Research. C.T. and L.T. are supported by the grant Progetti Premiali 2012 iALMA (CUP C52I13000140001), and D.F. from project SIR (RBSI14ZRHR); L.T. acknowledges the Deutsche Forschungsgemeinschaft (DFG; German Research Foundation)—ref No. FOR 2634/1ER685/11-1 and the DFG cluster of excellence ORIGINS (www.origins-cluster.de). G.L. and L.T. received funding from the EU Horizon 2020 research and innovation programme, Marie Sklodowska-Curie grant agreement 823823 (Dustbusters RISE project). C.P. acknowledges funding from the Australian Research Council via FT170100040 and DP180104235 and from ANR of France (ANR-16-CE31-0013). This Letter makes use of the following ALMA data: ADS/JAO.ALMA 2013.1.00592.S. ALMA is a partnership of ESO (representing its member states), NSF (USA)

and NINS (Japan), together with NRC (Canada), MOST and ASIAA (Taiwan), and KASI (Republic of Korea), in cooperation with the Republic of Chile. The Joint ALMA Observatory is operated by ESO, AUI/NRAO, and NAOJ.

ORCID iDs

Claudia Toci https://orcid.org/0000-0002-6958-4986
Giuseppe Lodato https://orcid.org/0000-0002-2357-7692
Davide Fedele https://orcid.org/0000-0001-6156-0034
Leonardo Testi https://orcid.org/0000-0003-1859-3070
Christophe Pinte https://orcid.org/0000-0001-5907-5179

References

Alexander, R., Pascucci, I., Andrew, S., Armitage, P., & Cieza, L. 2014, in Protostars and Planets VI, ed. H. Beuther et al. (Tucson, AZ: Univ. Arizona Press), 475
ALMA Partnership, Brogan, C. L., Pérez, L. M., et al. 2015, ApJL, 808, L3
Andrews, S. M., Huang, J., Pérez, L. M., et al. 2018, ApJL, 869, L41
Ballabio, G., Dipierro, G., Veronesi, B., et al. 2018, MNRAS, 477, 2766
Bate, M. R., Bonnell, I. A., & Price, N. M. 1995, MNRAS, 277, 362
Benisty, M., Juhasz, A., Boccaletti, A., et al. 2015, A&A, 578, L6
Bertrang, G. H.-M., Avenhaus, H., Casassus, S., et al. 2018, MNRAS, 474, 5105
Birnstiel, T., Andrews, S. M., Pinilla, P., & Kama, M. 2015, ApJL, 813, L14
Brauer, F., Dullemond, C. P., & Henning, Th. 2008, A&A, 480, 859
Crida, A., Morbidelli, A., & Masset, F. 2006, Icar, 181, 587
Dipierro, G., & Laibe, G. 2017, MNRAS, 469, 1932
Dipierro, G., Price, D., Laibe, G., et al. 2015, MNRAS, 453, L73
Draine, B. T. 2003, ApJ, 598, 1017
Fedele, D., Carney, M., Hogerheijde, M. R., et al. 2017, A&A, 600, A72
Fressin, F., Torres, G., Charbonneau, D., et al. 2013, ApJ, 766, 81
Gaia Collaboration, Brown, A. G. A., Vallenari, A., et al. 2016, A&A, 595, A2
Gonzalez, J.-F., Laibe, G., Maddison, S. T., Pinte, C., & Ménard, F. 2015, MNRAS, 454, L36
Gratton, R., Ligi, R., Sissa, A., et al. 2019, A&A, 623, A140
Honda, M., Maaskant, K., Okamoto, Y. K., et al. 2012, ApJ, 752, 143
Huang, J., Andrews, S. M., Cleeves, L. I., et al. 2018, ApJ, 822, 122
Isella, A., Benisty, M., Teague, R., et al. 2019, ApJL, 879, L25
Keppler, M., Benisty, M., Müller, A., et al. 2018, A&A, 617, A44
Laibe, G., & Price, D. J. 2014, MNRAS, 440, 2147
Ligi, R., Vigan, A., Gratton, R., et al. 2018, MNRAS, 473, 1774
Liu, Y., Dipierro, G., Ragusa, E., et al. 2019, A&A, 622, A75
Lodato, G., Dipierro, G., Ragusa, E., et al. 2019, MNRAS, 486, 453
Lodato, G., & Price, D. J. 2010, MNRAS, 405, 1212
Long, F., Pinilla, P., Herczeg, G. J., et al. 2018, ApJ, 869, 17
Macías, E., Espaillat, C. C., Osorio, M., et al. 2019, ApJ, 881, 159
Mordasini, C., van Boekel, R., Mollière, P., Henning, Th., & Benneke, B. 2016, ApJ, 832, 41
Osorio, M., Anglada, G., Carrasco-González, C., et al. 2014, ApJL, 791, L36
Panić, O., Hogerheijde, M. R., Wilner, D., & Qi, C. 2008, A&A, 491, 219
Pérez, S., Casassus, S., Baruteau, C., et al. 2019, AJ, 158, 15
Pinilla, P., Benisty, M., & Birnstiel, T. 2012, A&A, 545, A81
Pinilla, P., Flock, M., Ovelar, M. d. J., & Birnstiel, T. 2016, A&A, 596, A81
Pinte, C., Harries, T. J., Min, M., et al. 2009, A&A, 498, 967
Pinte, C., Ménard, F., Duchêne, G., & Bastien, P. 2006, A&A, 459, 797
Pinte, C., Price, D. J., Ménard, F., et al. 2018, ApJL, 860, L13
Pohl, A., Benisty, M., Pinilla, P., et al. 2017, ApJ, 850, 52
Price, D. J., Wurster, J., Tricco, T. S., et al. 2018, PASA, 35, e031
Reggiani, M., Quanz, S. P., Meyer, M. R., et al. 2014, ApJL, 792, L23
Shakura, N. I., & Sunyaev, R. A. 1973, A&A, 24, 337
Siess, L., Dufour, E., & Forestini, M. 2000, A&A, 358, 593
Suriano, S. S., Li, Z.-Y., Krasnopolsky, R., & Shang, H. 2018, MNRAS, 477, 1239
Testi, L., Skemer, A., Henning, Th., et al. 2015, ApJL, 812, L38